Global assessment of climatic responses to the ozone-vegetation interactions

Xinyi Zhou[1], Xu Yue[1], Chenguang Tian[1], Xiaofei Lu[1]

[1] Jiangsu Key Laboratory of Atmospheric Environment Monitoring and Pollution Control, Collaborative Innovation Center of Atmospheric Environment and Equipment Technology, School of Environmental Science and Engineering, Nanjing University of Information Science & Technology, Nanjing, 210044, China

Corresponding author: Xu Yue (Email: yuexu@nuist.edu.cn)

Abstract. The coupling between surface ozone (O_3) and vegetation significantly influences regional to global climate. O_3 uptake by plant stomata inhibits photosynthetic rate and stomatal conductance, impacting evapotranspiration through land surface ecosystems. Using a climate-vegetation-chemistry coupled model (the NASA GISS ModelE2 coupled with Yale Interactive terrestrial Biosphere, or ModelE2-YIBs), we assess the global climatic responses to O_3-vegetation interactions during boreal summer of the present day (2005-2014). High O_3 pollution reduces stomatal conductance, resulting in warmer and drier conditions worldwide. The most significant responses are found in the eastern U.S. and eastern China, where surface air temperature increases by +0.33±0.87 °C and +0.56±0.38 °C, respectively. These temperature rises are accompanied by decreased latent heat and increased sensible heat in both regions. The O_3-vegetation interaction also affects atmospheric pollutants. Surface maximum daily 8-hour average O_3 concentrations increase by +1.46±3.02 ppbv in eastern China and +1.15±1.77 ppbv in eastern U.S due to the O_3-induced inhibition of stomatal uptake. With reduced atmospheric stability following the warmer climate, increased cloudiness but decreased relative humidity jointly reduce aerosol optical depth by -0.06±0.01 (-14.67±12.15%) over eastern China. This study suggests that vegetation feedback should be considered for a more accurate assessment of climatic perturbations caused by tropospheric O_3.

1 Introduction

Tropospheric ozone (O_3), one of the most detrimental air pollutants (Myhre et al., 2013), not only poses threats to human health (Norval et al., 2011; Nuvolone et al., 2018) but also induces phytotoxic effects to vegetation (Mills et al., 2007; Pleijel et al., 2007). When exposed to certain levels of O_3, plant photosynthesis and stomatal conductance is inhibited due to the O_3 oxidation of cellular, enzyme, and chlorophyll (Dizengremel, 2001; Fiscus et al., 2005; Jolivet et al., 2016). Consequently, the carbon assimilation of terrestrial ecosystems is limited (Yue and Unger, 2014; Oliver et al., 2018) and the land-air exchange rates of water and heat fluxes are altered (Lombardozzi et al., 2015).

Experimental studies have shown that the excessive O_3 exposure reduced both plant photosynthesis and stomatal conductance (Ainsworth et al., 2012; Lombardozzi et al., 2013). The reduction rates are dependent on the O_3 stomatal fluxes as well as the damaging sensitivities that vary among different vegetation types (Nussbaum and Fuhrer, 2000; Karlsson et al., 2004; Pleijel et al., 2004). Several exposure-based indexes such as accumulated hourly O_3 concentrations over a threshold of 40 ppb (AOT40) and sum of all hourly average concentrations (SUM00) are used to assess O_3-induced vegetation damage (Fuhrer et al., 1997; Paoletti et al., 2007). In addition, the flux-related POD_y method (phytotoxic O_3 dose above a threshold flux of y) is also widely applied to consider the dynamic adjustment of stomatal conductance (Buker et al., 2015; Sicard et al., 2016). Taking into account the variability of plant sensitivities, different O_3 damage schemes were proposed to quantify the O_3 impacts on land carbon assimilation from regional to global scales (Anav et al., 2011; Lam et al., 2023; Lei et al., 2020). For example, Sitch et al. (2007) calculated the simultaneous damages to both photosynthesis and stomatal conductance based on the instantaneous O_3 stomatal uptake. In contrast, Lombardozzi et al. (2012) estimated the decoupled reductions in plant photosynthesis and stomatal conductance using different response relationships to the cumulative O_3 stomatal uptake. Applications of different schemes resulted in a wide range of reductions in gross primary productivity (GPP) by 2-12% globally with regional hotspots up to 20-30% (Lombardozzi et al., 2015; Unger et al., 2020; Zhou et al., 2024).

The O_3-induced inhibition in stomatal conductance decreases dry deposition and consequently enhances surface O_3 concentrations (Clifton et al., 2020; Wesely and Hicks, 2000; Zhang et al., 2006). Using the Sitch et al. (2007) scheme with high O_3 damaging sensitivities in the ModelE2-YIBs (NASA GISS ModelE2 coupled with Yale Interactive terrestrial Biosphere model), Gong et al. (2020) revealed that O_3-vegetation interactions increased regional O_3 concentrations by 1.8 ppbv in the eastern U.S., 1.3 ppbv in Europe, and 2.1ppbv in eastern China for the year 2010. As a comparison, Sadiq et al. (2017) found consistently stronger feedback on O_3 concentrations in these polluted regions using the scheme of Lombardozzi et al (2012) embedded in the Community Earth System Model (CESM). Moreover, the inclusion of online O_3-vegetation interactions in numerical models will also result in a greater loss of simulated land carbon assimilation due to the feedbacks of both ecosystems and surface O_3. This is attributable to several factors. On one hand, O_3 damages to leaf photosynthesis inhibit plant growth and decrease leaf area index (LAI), leading to higher reduction percentage in GPP compared to simulations without LAI changes (Yue et al., 2020). On the other hand, the O_3 enhancement due to vegetation feedback may cause additional vegetation damage and result in further GPP losses (Lei et al., 2021). As a result, the O_3-vegetation interactions should be considered in the global estimate of O_3 damages to ecosystem functions.

In addition to affecting surface O_3, the O_3-vegetation interaction can also alter the water and energy exchange between land and atmosphere through the modulation of stomatal conductance. For example, Lombardozzi et al. (2015) used the Community Land Model (CLM) and estimated that the cumulative uptake of O_3 by the leaves resulted in reduction of 2.2% in transpiration but increase of 5.4% in runoff globally. Arnold et al. (2018) used CESM and found that plant exposure to O_3 could decrease the land-air moisture fluxes and atmospheric humidity, which further reduced shortwave cloud forcing in polluted regions and induced widespread surface warming up to +1.5 K. Two recent studies utilized the WRF-chem model and revealed considerable warming and the associated meteorological perturbations due to the O_3-vegetation interactions in China (Zhu et al., 2022; Jin et al., 2023). However, all these modeling

studies applied the same O_3 vegetation damage scheme proposed by Lombardozzi et al. (2012). It's necessary to assess the climatic responses to O_3-vegetation interactions using different schemes so as to explore the robust responses and the associated uncertainties.

In this study, we quantified the global impacts of O_3-vegetation interaction on climatic conditions and surface air pollutants during 2010s using the ModelE2-YIBs (Yue and Unger, 2015). This fully coupled framework was implemented with the semi-mechanistic O_3 damage scheme proposed by Sitch et al. (2007), which calculated aggregated O_3 damage to photosynthesis based on varied sensitivities to instantaneous stomatal O_3 uptake across eight plant functional types (PFTs). We performed sensitivity experiments to quantify the responses of surface air temperature and precipitation to O_3-vegetation interaction. The feedbacks to aerosols and O_3 concentrations were also examined.

2 Method

2.1 Model descriptions

The ModelE2-YIBs is a fully coupled climate-carbon-chemistry model combining the NASA GISS ModelE2 with the YIBs vegetation model. ModelE2 is a general circulation model with the horizontal resolution of 2°×2.5° in latitude and longitude and 40 vertical layers up to 0.1 hPa. It dynamically simulates gas-phase chemistry (NO_x - HO_x - O_x - CO - CH4 - NMVOCs), aerosols (sulfate, nitrate, black and organic carbon, dust, and sea salt), and their interactions (Menon and Rotstayn, 2006). Both the physical and chemical processes are calculated every 0.5 h and the radiation module is called every 2.5 h. The radiation module includes direct and indirect aerosol radiative effects and accounts for absorption of multiple greenhouse gases (GHGs). For cloud optical parameters, it uses Mie scattering, ray tracing, and matrix theory (Schmidt et al., 2006). The model outperforms 20 other IPCC-class climate models in simulating surface solar radiation (Wild et al., 2013) and has been extensively validated for meteorological and hydrological variables against observations and reanalysis data (Schmidt et al., 2014).

The YIBs model employs the well-established Farquhar model for leaf

photosynthesis and Ball-Berry model for stomatal conductance (Farquhar et al., 1980; Ball et al., 1987) as follows:

$$A_{tot} = \min(J_c, \quad J_e, \quad J_s) \tag{1}$$

Here, the total leaf photosynthesis, denoted as A_{tot} (μmol m^{-2} [leaf] s^{-1}), is calculated considering both C_3 (Collatz et al., 1991) and C_4 plants (Collatz et al., 1992). The A_{tot} is derived from the minimum value of the constraints. The ribulose-1,5-bisphosphate carboxylase (Rubisco) limited rate of carboxylation is J_c:

$$J_c = \begin{cases} V_{cmax}\left(\dfrac{c_i - \Gamma_*}{c_i + K_c(1 + O_i/K_o)}\right) & \text{for } C_3 \text{ plant} \\ V_{cmax} & \text{for } C_4 \text{ plant} \end{cases} \tag{2}$$

The carboxylation rate restricted by the availability of light is J_e:

$$J_e = \begin{cases} a_{leaf} \times PAR \times \alpha \times \left(\dfrac{c_i - \Gamma_*}{c_i + 2\Gamma_*}\right) & \text{for } C_3 \text{ plant} \\ a_{leaf} \times PAR \times \alpha & \text{for } C_4 \text{ plant} \end{cases} \tag{3}$$

The export-limited rate for C_3 plants and the phosphoenolpyruvate carboxylase (PEPC) limited rate of carboxylation for C_4 plants are represented by J_s:

$$J_s = \begin{cases} 0.5\, V_{cmax} & \text{for } C_3 \text{ plant} \\ K_s \times V_{cmax} \times \dfrac{c_i}{P_{atm}} & \text{for } C_4 \text{ plant} \end{cases} \tag{4}$$

In these functions, V_{cmax} (μmol m^{-2} s^{-1}) is the maximum carboxylation capacity. c_i and O_i (Pa) represent the internal leaf CO_2 and oxygen partial pressure. Γ_* (Pa) denotes the CO_2 compensation point, while K_c and K_o (Pa) are Michaelis–Menten constants for the carboxylation and oxygenation of Rubisco, respectively. The parameters Γ_*, K_c, and K_o vary with temperature based on the sensitivity of the vegetation to temperature (Q_{10} coefficient). PAR (μmol m^{-2} s^{-1}) is the absorbed photosynthetically active radiation, a_{leaf} is leaf-specific light absorbance that considers sunlit and shaded leaves, and α is quantum efficiency. P_{atm} (Pa) represents the ambient pressure. K_s is set to 4000 as a constant following Oleson et al. (2010), to limit photosynthesis of C_4 plants get saturated at lower CO_2 concentrations.

$$g_s = m\,\frac{(A_{tot} - R_d) \times RH}{c_s} + b \tag{5}$$

The stomatal conductance (g_s, mol [H_2O] m^{-2} s^{-1}) is linked to the variations of A_{tot} with parameters such as dark respiration rate (R_d, μmol m^{-2} s^{-1}), relative humidity (RH),

and CO_2 concentration at the leaf surface (c_s). The model simulates the biophysical processes of eight PFTs including tundra, C_3/C_4 grass, shrubland, deciduous broadleaf forest, evergreen broadleaf forest, evergreen needleleaf forest, and cropland. Different values are assigned to parameters *m* and *b* for each PFT (Table S1). The carbon uptake by the leaf is then accumulated and allocated to different organs to support the plant development with dynamical changes in LAI and tree growth.

2.2 The O_3-vegetation damage scheme

The YIBs model employs a semi-mechanistic parameterization proposed by Sitch et al. (2007) to estimate the impact of O_3 on photosynthesis through stomatal uptake. The scheme applies an undamaged factor (F) (nmol m^{-2} s^{-1}) to both A_{tot} and g_s as follows:

$$A_{totd} = A_{tot} \cdot F \quad (6)$$

$$g_{sd} = g_s \cdot F \quad (7)$$

where A_{totd} and g_{sd} are the unaffected photosynthesis and stomatal conductance separately. The factor *F* is defined as:

$$F = 1 - a_h \cdot \max\left[F_{O3} - F_{O3,crit}, 0.0\right] \quad (8)$$

a_h (mmol m^{-2} s^{-1}) is the high O_3 sensitivity coefficient, calibrated by Sitch et al. (2007) on data from field observations by Karlsson et al. (2004) and Pleijel et al. (2004) to represent 'high' sensitivity of relative species of each PFT. $F_{O3,crit}$ (nmol m^{-2} s^{-1}) is the specific threshold for O_3 damages, both of which varies with vegetation types (Table S1).

$$F_{O3} = \frac{[O_3]}{R_a + [\frac{k_{O3}}{g_{sd}}]}, \quad (9)$$

where $[O_3]$ represents surface O_3 concentrations, R_a (s m^{-1}) stands for aerodynamic resistance, which expresses turbulent transport efficiency in transferring sensible heat and water vapor between the land surface and a reference height. The constant k_{O3}=1.67 is the ratio of stomatal resistance for O_3, estimated based on the theoretical stomatal resistance to water (Laisk et al., 1989). When plants are exposed to [O_3] (Eq. 9), A_{tot} and g_s will decrease (Eq. 6 and Eq. 7) if the excess O_3 enters leaves (Eq. 8).

The increased stomatal resistance acts to protect plants by reducing the O_3 uptake of stomata. Consequently, the damage scheme describes both changes in photosynthetic rate and stomatal conductance.

2.3 Experiments

To explore the coupled O_3-vegetation effect, we performed two simulations using the ModelE2-YIBs model. The control experiment "O3_offline" was conducted without the O_3 damages to vegetation. As a comparison, the sensitivity experiment "O3_online" contained online O_3-vegetation interaction with high O_3 sensitivity. For both experiments, the anthropogenic emissions of 2010 (the average of 2005-2014) for 8 species (BC, OC, CO, NH_3, NO_x, SO_2, Alkenes, and Paraffin) from 8 economic sources (agriculture, energy, industry, transportation, resident, solvent, waste, and international shipping) and biomass burning source were collected from the Coupled Model Intercomparison Project phase 6 (CMIP6) (van Marle et al., 2017; Hoesly et al., 2018). The ensemble mean of monthly sea surface temperature (SST) and sea ice fraction (SIC) simulated by 21 CMIP6 models during the time period 2005-2014 was employed as the boundary conditions. The cover fraction of 8 PFTs (Fig. S1) fixed at 2010 were adopted from the land use harmonization (LUH2) dataset (Hurtt et al., 2020). For each time-slice simulation, the model was run for 30 years with all the input data fixed and the first 10 years are used as the spin up. We calculated the average of the last 20 years and focused on the boreal summer season (June-July-August, JJA) when the interaction of vegetation and surface O_3 reaches the maximum in one year (fig. S3). In order to show the uncertainty introduced by the internal variability of the model, all the related global/regional values are denoted as "mean/sum ± standard deviation of the last 20 model years". We explored the climatic responses to O_3-vegetation interactions as the differences between "O3_online" and "O3_offline" on the global scale with the focus over the hotspot regions such as eastern U.S. (30–40º N, 80–90 º W) and eastern China (22.5–38º N, 106–122º E).

2.4 Data for model evaluation

We evaluated the simulated air pollutants, carbon fluxes, and meteorological variables from 'O3_offline' run using observational and reanalysis datasets. The worldwide observations of the maximum daily 8-hour average O_3 (MDA8 O_3) concentrations were mainly collected from three regional networks: Air Quality Monitoring Network operated by Ministry of Ecology and Environment (AQMN-MEE) in China, the Clean Air Status and Trends Network (CASTNET) in the U.S., and the European Monitoring and Evaluation Programme (EMEP) in Europe. Observations used for validation beyond China, sourced from Sofen et al. (2016), are averaged over the period 2005-2014. This dataset encompasses 7288 station records worldwide and excludes the uncertainty associated with high mountain-top sites. For AQMN-MEE, the mean value of 2014-2018 was used due to its establishment in 2013. The simulated aerosol optical depth (AOD) and LAI were validated using satellite-based data from the Moderate Resolution Imaging Spectroradiometer (MODIS) retrievals collection 5 (Remer et al., 2005) (http://modis.gsfc.nasa.gov/) averaged for the years 2005-2014. The simulated GPP was evaluated against the data product upscaled from the FLUXNET eddy covariance measurements for 2009-2011 (Jung et al., 2011). The daily temperature at 2m (T_{2m}) in 2005-2014 was obtained from the National Centers for Environmental Prediction/National Center for Atmospheric Research (NCEP/NCAR) reanalysis 1 (NCEP1) (Kalnay et al., 1996). For precipitation, we used the monthly data averaged in 2005-2014 from Global Precipitation Climatology Project (GPCP) (Huffman et al., 1997; Adler et al., 2018). All these datasets were interpolated to the same resolution as ModelE2-YIBs model. Root-mean-square-error (RMSE) and normalized mean biases (NMBs) were applied to quantify the deviations of simulations from observations:

$$RMSE = \sqrt{\frac{1}{n}\sum_{i=1}^{n}(S_i - O_i)^2} \quad (10)$$

$$NMB = \sum_{i=1}^{n}(S_i - O_i)/\sum_{i=1}^{n} O_i \times 100\% \quad (11)$$

Here, S_i and O_i represent the simulated and observed values, respectively. *n* denotes the total grid number used in the comparisons.

3. Results

3.1 The control simulation and model evaluations

We first evaluated the air pollutants simulated by the control simulation O3_offline of ModelE2-YIBs model (Fig. 1). Over a total of 503 grids with site-level O_3 measurements (Fig. 1b), the model replicated both the magnitude and spatial distribution of MDA8 O_3, with correlation coefficient (r) of 0.59 and NMB of -2.54% (Fig. 1c). Simulated summertime surface MDA8 O_3 was high in regions with large anthropogenic emissions, such as western Europe and eastern China (Ohara et al., 2007), as well as in central Africa with frequent fire emissions (van der Werf et al., 2017). On the global scale, the model yielded an average MDA8 O_3 of 43.93 ppbv and observations showed an average of 44.72 ppbv over the same grids. However, the modeled result is overestimated over the North China Plain and slightly underestimated over the U.S., likely due to the biases in the emission inventories and predicted climate that drive the O_3 production. Simulated AOD at 550 nm by O3_offline (Fig. 1d) showed similar spatial pattern as the satellite retrievals (Fig. 1e) with R=0.75 and NMB of -7.35% globally (Fig. 1f). Both the simulations and observations showed AOD hotspots over North Africa and the Middle East where dust emissions dominate, and in northern India and eastern China where anthropogenic emissions are large (Feng et al., 2020).

We then evaluated the simulated GPP and LAI by the control experiment for the boreal summer period (Fig. 2). Observations showed GPP hotspots over boreal forests such as eastern U.S., Eurasia, and East Asia and the tropical forests such as Amazon, central Africa, and Indonesia (Fig. 2b). The seasonal total GPP was estimated to be 41.63Pg[C], which accounted for 35% of the annual amount. Simulations captured the observed GPP pattern on the global scale, with r = 0.64 and NMB = -7.81% over 2581 grids (Fig. 2c), with underestimation in the tundra area and slight overestimation in the tropical rain forest and evergreen forest regions. The model simulated a seasonal total GPP of 38.69 Pg[C], equivalent to 34% of the annual amount. Simulated LAI showed similar patterns as GPP (Fig. 2d) and resembled observed LAI (Fig. 2e) with a spatial correlation r = 0.79 and a low NMB = -5.43% over 4435 grids globally (Fig. 2f).

We further validated the simulated meteorology from O3_offline (Fig. S2). For

surface air temperature, the model (Fig. S2a) reproduced observed (Fig. S2b) pattern with RMSE of 3.21 °C and r of 0.99 against observations (Fig. S2c). For precipitation, the simulation (Fig. S2d) captures the observed spatial pattern (Fig. S2e) with NMB = 17.26% and r = 0.75 (Fig. S2f). Overall, the model captures the spatial characteristics and magnitudes of air pollutants, biospheric parameters, and meteorological fields, making it a valuable tool for studying O_3-vegetation interactions.

3.2 O_3 damage to terrestrial ecosystems

We assessed the damaging effects of surface O_3 to ecosystems due to online O_3-vegetation interactions (Fig. 3). The impacts of O_3 on biospheric variables were mainly located in regions characterized by abundant vegetation cover and elevated O_3 concentrations. On the global scale, O_3 induced the GPP reduction of -1.80±0.61 PgC yr^{-1} (-4.69±1.56%, Fig. 3a). This deleterious effect was more pronounced in specific regions, notably eastern China and eastern U.S., with significant GPP declines of -25.40±1.90% and -20.14±5.02%, respectively, under high O_3 sensitivity conditions (Fig. 3a and Table S2). Meanwhile, stomatal conductance significantly decreased in the middle latitudes of Northern Hemisphere (Fig. 3b). The most substantial relative change of -30.62±4.30% was observed in eastern China, followed by -25.65±9.32% in the eastern U.S. (Fig. 3b and Table S2). Though there are positive responses in some regions, they are not dominant and hardly significant. These values were stronger than that for GPP (Fig. 3a), likely due to the climatic feedback to O_3-vegetation interactions. The opening of plant stoma plays a crucial role in regulating the energy and water exchange between land surface and the atmosphere. The inhibition of stomatal conductance by surface O_3 leads to the warmer (Fig. 4a) and drier (Fig. 4b) climate in those hotspot regions, resulting in even stronger inhibition effects on stomatal conductance. Following the changes in GPP, global LAI on average decreased by 0.01±0.01 m^2 m^{-2} (-0.62±0.84%) with regional maximums of -4.53±1.14% in eastern China and -5.87±3.11% in eastern U.S. (Table S2).

3.3 Global climatic responses to O_3-vegetation interactions

In response to the O_3-induced inhibition of stomatal conductance, surface air temperature increased by 0.05±0.20°C (Fig. 4a) while precipitation decreased by -0.01±0.03 mm day^{-1} (Fig. 4b) on the global scale. The most significant change was the warming of 0.56±0.38°C and precipitation reduction of -0.79±1.05 mm day^{-1} (-16.18±20.38%) in eastern China (Table S3), following the largest inhibition to stomatal conductance (Fig. 3b). Such warming and rainfall deficit also appeared in eastern U.S. and western Europe, where the O_3-vegetation interactions were notable. The O_3-induced inhibition to stomatal conductance decreased latent heat flux (Fig. 4e) and the consequent precipitation (Fig. 4b) in those hotspot regions. Meanwhile, the reduction of latent heat flux promotes surface air temperature (Fig. 4a), resulting in the increase of sensible heat flux (Fig. 4f). Such warming was also reported in field experiments, where relatively high O_3 exposure resulted in noticeable increases of canopy temperature along with reductions of transpiration (Bernacchi et al., 2011; VanLoocke et al., 2012). Globally, temperature and precipitation showed patchy responses with both positive and negative anomalies, suggesting that the regional hotspots of O_3-induced meteorological changes propagate to surrounding areas through atmospheric perturbations.

We further examined the changes in air humidity and cloudiness. Surface relative humidity decreased by -0.18±0.53% globally with a similar pattern as that of precipitation (Fig. 4c). The most significant reductions were over eastern China and eastern U.S., where both the warming (Fig. 4a) and rainfall deficit (Fig. 4b) contributed to the drought. However, in the adjacent regions such as northern China and central U.S., both rainfall and surface relative humidity showed certain enhancement. These changes were associated with the regional increase of cloud cover (Fig. 4d). The sensible heat flux increased by 6.3±5.4 W m^{-2} (16.54±15.59%) and 7.12±3.86 W m^{-2} (25.46±14.71%) in eastern U.S. and eastern China, respectively, suggesting a transfer of thermal energy from land to the atmosphere by O_3-vegetation interactions (Fig. 4f and Table S3). The warming effect further triggered anomalous updrafts in the lower troposphere, represented by the changes in vertical velocity (Fig. 5), leading to

enhanced convection, reduced atmospheric stability, and consequently an increase in low-level cloudiness (Fig. 4d). However, despite the usual cooling effect associated with increased cloud cover due to reductions in radiation, in regions predominantly influenced by O_3-vegetation interactions, this cooling effect was outweighed by the O_3-induced warming through inhibition of stomatal conductance. Therefore, temperatures exhibited an overall increase of 0.56±0.38°C in eastern China and 0.33±0.87 °C in the eastern U.S. (Table S3).

3.4 Changes of air pollution by O_3-vegetation interactions

Changes in surface water and heat fluxes induced by O_3-vegetation interactions could feed back to affect air pollutants such as O_3 and aerosols. As Fig. 6a and Table S4 show, surface MDA8 O_3 concentrations enhanced 1.46±3.02 ppbv in eastern China and 1.15±1.77 ppbv in eastern U.S. due to the decreased dry deposition following O_3 inhibition on stomatal conductance. It indicates that the high contemporary O_3 pollution may worsen air quality through O_3-vegetation interactions. However, negative O_3 changes were predicted in central U.S. and western China, where the increased rainfall dampened O_3 through chemical reactions and wet deposition. On a global scale, surface MDA8 O_3 showed a limited increase of 0.03±0.4 ppbv due to the offset between positive and negative feedbacks. The enhancement of O_3 concentrations in polluted regions may exacerbate the warming effect of O_3 as a greenhouse gas and cause additional damages to vegetation. For instance, offline O_3 damages on GPP in eastern China and the eastern US are -0.52±0.03 Pg[C] (-24.98±0.91%) and -0.17±0.02 Pg[C] (-16.71±1.16%), respectively, smaller than those induced by O_3-vegetation interactions (Table S2).

Aerosols also exhibited evident changes by the O_3-vegetation interactions. The AOD showed significant reductions over the hotspot regions such as eastern China and eastern U.S. (Fig. 6b). In the ModelE2-YIBs model, sulfate was especially sensitive to cloud which could enhance the aerosol scavenging through cloud water precipitation (Koch et al., 2006). The large enhancement of cloudiness removed sulfate more efficiently than other aerosol species, leading to an average decline of -1.94±1.67 μg

m^{-3} (-8.52±6.88%) in $PM_{2.5}$ loading over eastern China (Fig. S4 and Table S4). Meanwhile, the reduction of surface relative humidity (Fig. 4c) in the regions with strong O_3-vegetation interactions limited the hygroscopic growth of aerosols, leading to a more noticeable decrease in AOD (Petters and Kreidenweis, 2007; Pitchford et al., 2007) by -0.06±0.05 (-14.67±16.75%) in eastern China (Table S4). The similar aerosol changes were found in eastern U.S. but with smaller reductions of $PM_{2.5}$ by -0.27±0.36 μg m^{-3} (-6.01±7.9%) and AOD by -0.01±0.01 (-8.15±9.38%) (Table S4). Beyond the key O_3-vegetation coupling regions, positive but insignificant changes in AOD were predicted, leading to the moderate AOD changes on the global scale (Fig. 6b).

4. Discussion and conclusions

We examined the O_3-vegetation feedback to climate and air pollution in the 2010s using the fully coupled climate-carbon-chemistry model ModelE2-YIBs. During boreal summer, surface O_3 resulted in strong damages to GPP and inhibitions to stomatal conductance with regional hotspots over eastern China and eastern U.S. Consequently, surface transpiration was weakened, leading to decreased latent heat fluxes and relative humidity but increased surface air temperature. Meanwhile, the surface warming increased cloud cover by reducing atmospheric stability. However, the enhancement of cloudiness decreased surface temperature and promoted precipitation outside the key regions with intense O_3-vegetation interactions. The O_3-induced inhibition to stomatal conductance resulted in a localized increase in O_3 concentrations. In contrast, the increased cloud cover and decreased relative humidity jointly reduced AOD in hotspot regions. On the global scale, the mean changes of both climate and air pollution were moderate due to the offset between the changes with opposite signs.

Our predicted changes in water/heat fluxes by O_3-vegetation interactions were consistent with previous studies (Lombardozzi et al., 2015; Arnold et al., 2018; Gong et al., 2020). For example, the simulations by Lombardozzi et al. (2015) revealed that surface O_3 reduces global GPP by 8%-12% and transpiration by 2-2.4% with regional reductions up to 20% for GPP and 15% for transpiration in eastern China and U.S. These changes were in general consistent with our results though we predicted larger

reductions in transpiration than GPP due to O_3-vegetation interactions. Using the same scheme as Lombardozzi et al. (2015), Sadiq et al. (2017) showed that O_3-vegetation coupling induced the surface warming of 0.5-1°C and O_3 enhancement of 4-6 ppbv in eastern China and eastern U.S. The magnitude of these responses was much stronger than our predictions, likely because they considered the accumulation effect of O_3. In contrast, the regional simulations by Jin et al. (2023) revealed that O_3-vegetation coupling led to the increases of temperature up to 0.16°C and surface O_3 up to 0.6 ppbv in eastern China, both of which were smaller than our predictions. The damage scheme they use, which depends on cumulative O_3 uptake, omits the difference in impact on sunlit or shaded leaves and will overestimate the O_3 damage on GPP compared to the scheme we use, which considers transient O_3 flux (Cao et al., 2024). The discrepancies of O_3-vegetation feedback using the same O_3 damage schemes revealed the uncertainties from climate and chemistry models. Our predictions were within the range of previous estimates for both climatic and O_3 changes.

There were some limitations in our simulated O_3-vegetation interactions. First, the semi-mechanistic O_3 damage scheme we used in the study linked the damages to photosynthesis with those to stomatal conductance (Sitch et al., 2007), leading to stronger inhibition percentage in stomatal conductance than that in photosynthesis considering the O_3-vegetation feedback. However, some observations showed that the damage to stomatal conductance occurred more slowly and might not be proportional to the decline of photosynthetic rates (Gregg et al., 2006; Lombardozzi et al., 2012). Second, observations have shown large variability of plant sensitivities to O_3 damages. The Sitch et al. (2007) scheme employed the low to high ranges of sensitivity to indicate the inter-specific variabilities. In this study, we employed only the high O_3 sensitivity to explore the maximum responses. The possible uncertainties due to varied O_3 damage sensitivities deserved further investigations. Third, large-scale observations were not available to validate the simulated regional to global responses of climate and air pollutants. The O_3 vegetation damage scheme was extensively validated against site-level measurements of both photosynthesis (Yue and Unger, 2018) and stomatal

conductance (Yue et al., 2016). However, we were conservative about the derived global responses given that previous studies showed large discrepancies using the same O_3 damage scheme but implemented in different climate and/or chemistry models (Lombardozzi et al., 2015; Sadiq et al., 2017; Jin et al., 2023). Furthermore, the 2°×2.5° resolution of current ModelE2-YIBs has limitation due to the high computational demands. However, high-resolution models exhibit improved simulations of extreme events (Chang et al., 2020; Ban et al., 2021), which have certain effect on O_3-vegetation interactions (Mills et al., 2016; Lin et al., 2020). While chemical transport models with relatively coarse resolution can raise biases in simulated air pollutants, they still capture large-scale patterns similar to fine-resolution results and is reasonable compared to observational data (Wang et al., 2013; Li et al., 2016; Lei et al., 2020). Moreover, we omit the slow climatic feedback caused by air-sea interaction in the simulations. Studies have revealed that these interactions may result in different climatic perturbations from those simulations with fast responses of land surface alone (Yue et al., 2011). A dynamic ocean model is considered to enrich the future research. Meanwhile, this study does not isolate the different impacts of aerosols, even though the radiation module includes both direct and indirect radiative effects. We will investigate this further in the future by identifying the main processes.

Despite these uncertainties, our simulations revealed considerable changes of both climate and air pollutants in response to O_3-vegetation interactions. The most intense warming, dryness, and O_3 enhancement were predicted in eastern China and eastern U.S., affecting the regional climate and threatening public health for these top two economic centers. In contrast, we for the first time revealed the reduction of aerosol loading in those hotspot regions, suggesting both positive and negative effects to air pollutants by O_3-vegetation feedback. Such interactions should be considered in the Earth system models so as to better project future changes in climate and air pollutants following the anthropogenic interventions to both O_3 precursor emissions and ecosystem functions.

Data Availability

The observational data and model outputs that support the findings in this study are available from corresponding authors upon reasonable request.

Author contributions

XY conceived the project. XZ performed the model simulations, conducted results analysis and wrote the draft manuscript. XY, CT and XL assisted in the interpretation of the results and contributed to the discussion and improvement of the paper.

Competing interests

The authors declare that they have no conflict of interest.

Acknowledgments

This study was jointly funded by National Key Research and Development Program of China (no. 2023YFF0805404) and National Natural Science Foundation of China (no. 42293323).

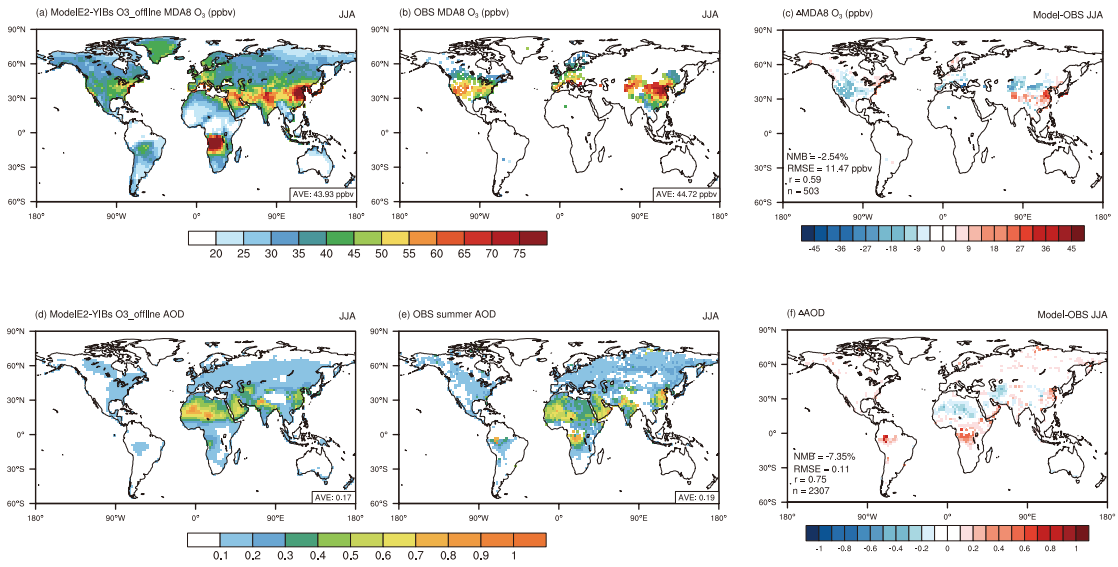

Figure 1. Evaluation of the boreal summertime (June-August) air pollutants at the present day simulated by the ModelE2-YIBs model. Surface daily maximum 8-hour ozone (MDA8 O_3; a-c) and aerosol optical depth (AOD; d-f) from the simulation O3_offline (a & d) and observations (b & e) are compared. The correlation coefficients (r), root mean square error (RMSE), normalized mean bias (NMB), and number of grid cells (n) for the comparisons are listed on the mean bias maps (c & f).

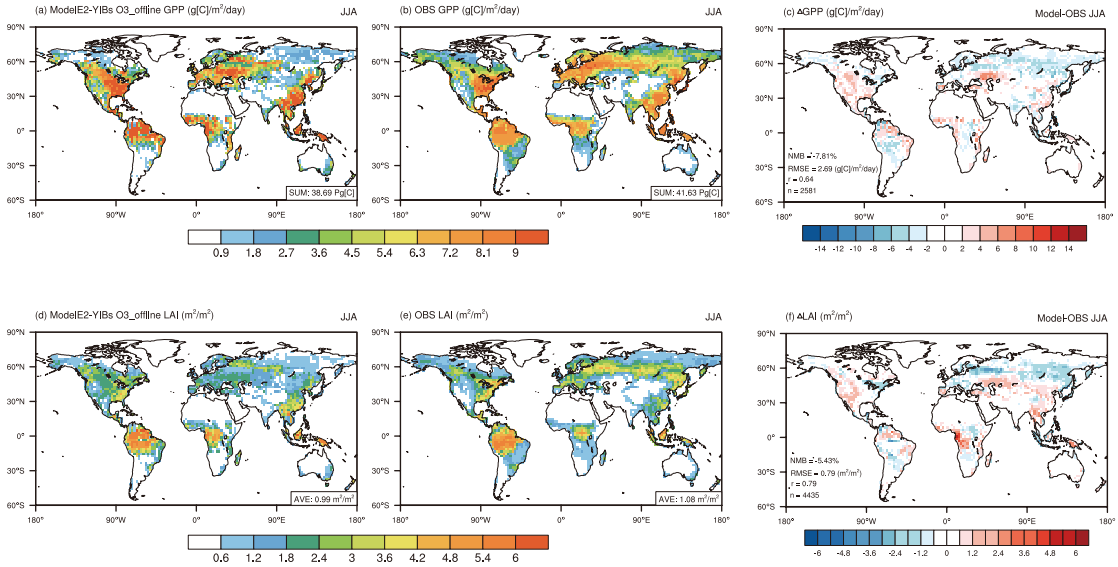

Figure 2. The same as Fig.1 but for gross primary productivity (GPP; a-c) and leaf area index (LAI; d-f).

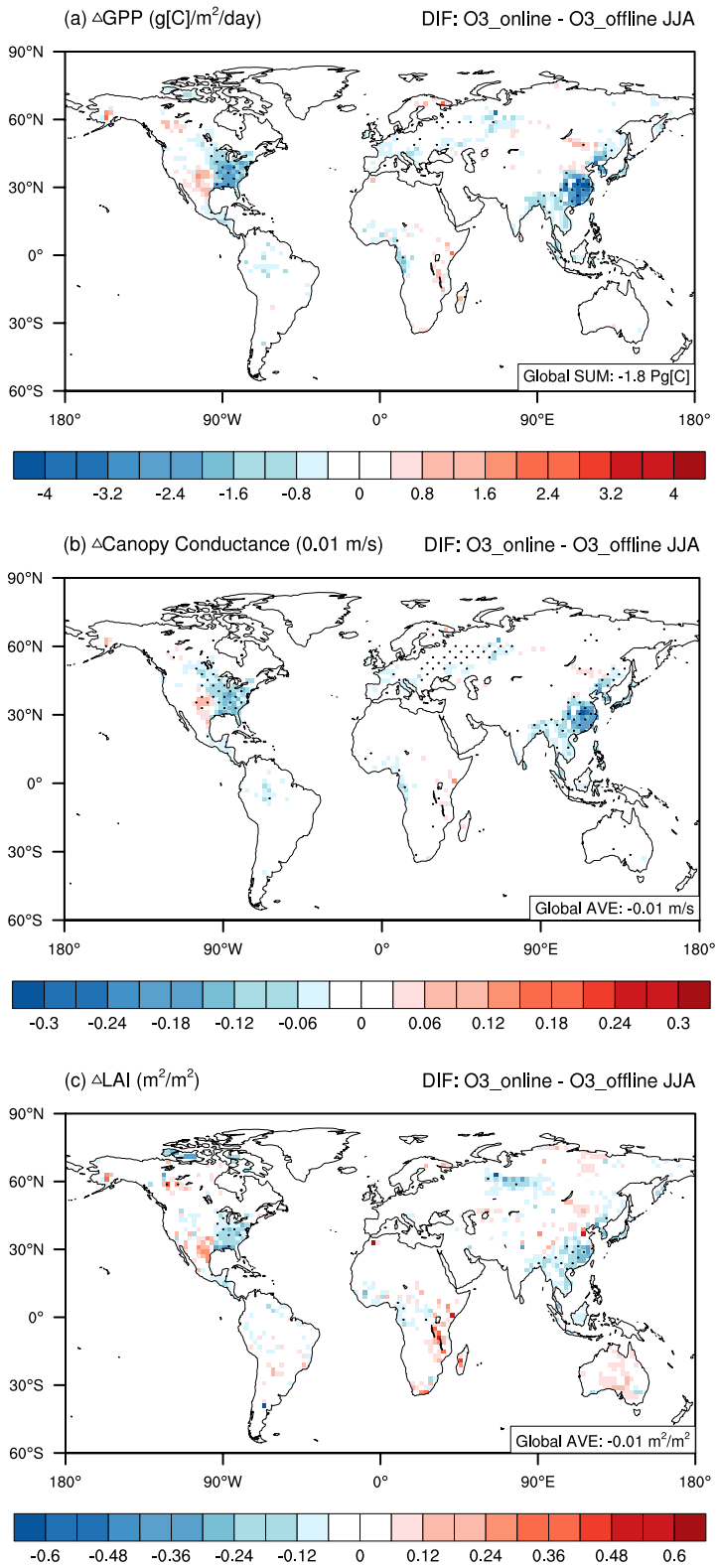

Figure 3. Changes of boreal summertime biospheric variables induced by O_3-vegetation interactions at the present day. Results shown are changes of (a) GPP, (b) canopy conductance, and (c) LAI between simulations O3_online and O3_offline. Black dots denote areas with significant changes ($p < 0.1$).

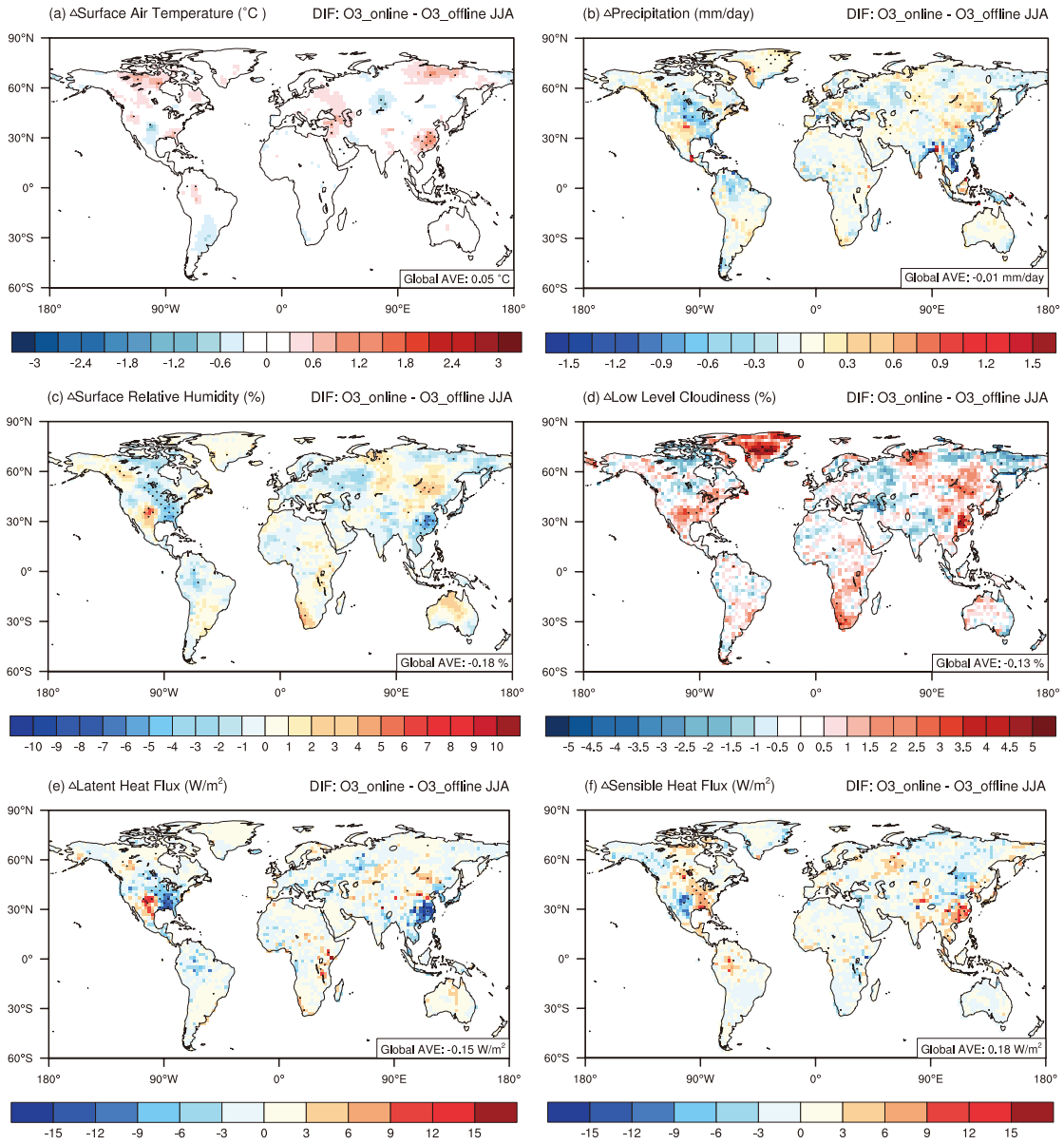

Figure 4. Changes of boreal summertime meteorological fields by O_3-vegetation interactions at the present day. Results shown are changes of (a) surface air temperature, (b) precipitation, (c) surface relative humidity, (d) low level cloudiness, (e) latent heat flux, and (f) sensible heat flux between simulations O3_online and O3_offline. For heat fluxes, positive values (shaded in red color) indicate the upward fluxes change. Black dots denote areas with significant changes ($p < 0.1$).

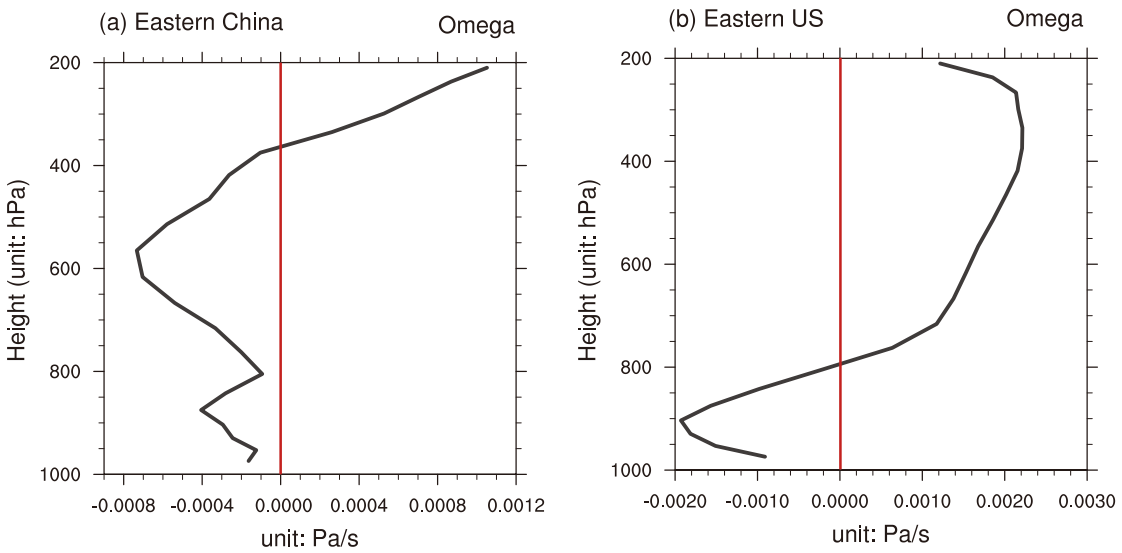

Figure 5. Vertical profile of vertical velocity. Results shown are changes of the vertical velocity in (a) Eastern China and (b) Eastern US between simulations O3_online and O3_offline. Solid red line denotes the value 0. Please notice the differences in the scales.

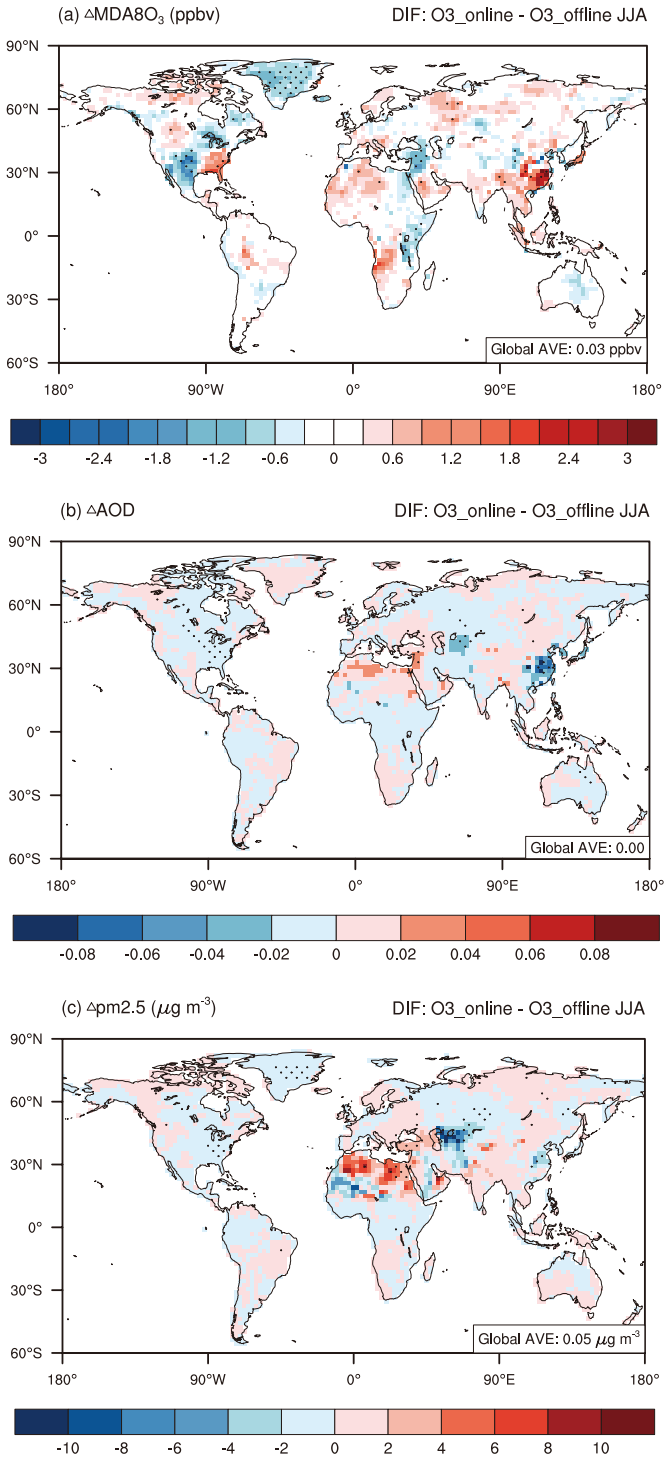

Fig. 6. Changes of summertime atmospheric pollution caused by O_3-vegetation interactions at present day. Results shown are changes of (a) O_3, (b) AOD, and (c) $PM_{2.5}$ between O3_online and O3_offline. Black dots denote areas with significant changes ($p < 0.1$).

References

Adler, R. F., Sapiano, M. R. P., Huffman, G. J., Wang, J.-J., Gu, G., Bolvin, D., Chiu, L., Schneider, U., Becker, A., Nelkin, E., Xie, P., Ferraro, R., and Shin, D.-B.: The Global Precipitation Climatology Project (GPCP) Monthly Analysis (New Version 2.3) and a Review of 2017 Global Precipitation, Atmosphere, 9, 138, https://doi.org/10.3390/atmos9040138, 2018.

Ainsworth, E. A., Yendrek, C. R., Sitch, S., Collins, W. J., and Emberson, L. D.: The effects of tropospheric ozone on net primary productivity and implications for climate change, Annu. Rev. Plant. Biol., 63, 637–661, https://doi.org/10.1146/annurev-arplant-042110-103829, 2012.

Anav, A., Menut, L., Khvorostyanov, D., and Viovy, N.: Impact of tropospheric ozone on the Euro-Mediterranean vegetation, Glob. Change. Biol., 17, 2342–2359, https://doi.org/10.1111/j.1365-2486.2010.02387.x, 2011.

Arnold, S. R., Lombardozzi, D., Lamarque, J. -F., Richardson, T., Emmons, L. K., Tilmes, S., Sitch, S. A., Folberth, G., Hollaway, M. J., and Val Martin, M.: Simulated Global Climate Response to Tropospheric Ozone-Induced Changes in Plant Transpiration, Geophys. Res. Lett., 45, 13070–13079, https://doi.org/10.1029/2018GL079938, 2018.

Ball, J. T., Woodrow, I. E., and Berry, J. A.: A Model Predicting Stomatal Conductance and its Contribution to the Control of Photosynthesis under Different Environmental Conditions, in: Progress in Photosynthesis Research, edited by: Biggins, J., Springer Netherlands, Dordrecht, 221–224, https://doi.org/10.1007/978-94-017-0519-6_48, 1987.

Ban, N., Caillaud, C., Coppola, E., Pichelli, E., Sobolowski, S., Adinolfi, M., Ahrens, B., Alias, A., Anders, I., Bastin, S. and Belušić, D.: The first multi-model ensemble of regional climate simulations at kilometer-scale resolution, part I: evaluation of precipitation, Clim. Dynam., 57, 275-302, https://doi.org/10.1007/s00382-021-05708-w, 2021.

Buker, P., Feng, Z., Uddling, J., Briolat, A., Alonso, R., Braun, S., Elvira, S., Gerosa, G., Karlsson, P. E., Le Thiec, D., Marzuoli, R., Mills, G., Oksanen, E., Wieser, G., Wilkinson, M., and Emberson, L. D.: New flux based dose-response relationships for ozone for European forest tree species, Environ. Pollut., 206, 163–174, https://doi.org/10.1016/j.envpol.2015.06.033, 2015.

Bernacchi, C. J., Leakey, A. D. B., Kimball, B. A., and Ort, D. R.: Growth of soybean at future tropospheric ozone concentrations decreases canopy evapotranspiration and soil water depletion, Environ. Pollut., 159, 1464–1472, https://doi.org/10.1016/j.envpol.2011.03.011, 2011.

Cao, J., Yue, X. and Ma, M.: Simulation of ozone-vegetation coupling and feedback in

China using multiple ozone damage schemes, Atmos. Chem. Phys., 24(7), 3973-3987, https://doi.org/10.5194/acp-24-3973-2024, 2024.

Chang, P., Zhang, S., Danabasoglu, G., Yeager, S.G., Fu, H., Wang, H., Castruccio, F.S., Chen, Y., Edwards, J., Fu, D. and Jia, Y.: An unprecedented set of high-resolution earth system simulations for understanding multiscale interactions in climate variability and change, J. Adv. Model. Earth. Sy., 12, https://doi.org/10.1029/2020MS002298, 2020.

Clifton, O. E., Paulot, F., Fiore, A. M., Horowitz, L. W., Correa, G., Baublitz, C. B., Fares, S., Goded, I., Goldstein, A. H., Gruening, C., Hogg, A. J., Loubet, B., Mammarella, I., Munger, J. W., Neil, L., Stella, P., Uddling, J., Vesala, T., and Weng, E.: Influence of Dynamic Ozone Dry Deposition on Ozone Pollution, J. Geophys. Res-Atmos, 125, e2020JD032398, https://doi.org/10.1029/2020JD032398, 2020.

Collatz, G. J., Ball, J. T., Grivet, C., and Berry, J. A.: Physiological and Environmental-Regulation of Stomatal Conductance, Photosynthesis and Transpiration – a Model That Includes a Laminar Boundary-Layer, Agr. Forest Meteorol., 54, 107–136, doi:10.1016/0168-1923(91)90002-8, 1991.

Collatz, G. J., Ribas-Carbo, M., and Berry, J. A.: Coupled Photosynthesis-Stomatal Conductance Model for Leaves of C4 Plants, Aust. J. Plant Physiol., 19, 519–538, https://doi.org/10.1071/PP9920519, 1992.

Dizengremel, P.: Effects of ozone on the carbon metabolism of forest trees, Plant. Physiol. Bioch., 39, 729–742, https://doi.org/10.1016/S0981-9428(01)01291-8, 2001.

Farquhar, G. D., von Caemmerer, S., and Berry, J. A.: A biochemical model of photosynthetic CO_2 assimilation in leaves of C_3 species, Planta, 149, 78–90, https://doi.org/10.1007/BF00386231, 1980.

Feng, L., Smith, S. J., Braun, C., Crippa, M., Gidden, M. J., Hoesly, R., Klimont, Z., van Marle, M., van den Berg, M., and van der Werf, G. R.: The generation of gridded emissions data for CMIP6, Geosci. Model Dev., 13, 461–482, https://doi.org/10.5194/gmd-13-461-2020, 2020.

Fiscus, E. L., Booker, F. L., and Burkey, K. O.: Crop responses to ozone: uptake, modes of action, carbon assimilation and partitioning, Plant. Cell. Environ., 28, 997–1011, https://doi.org/10.1111/j.1365-3040.2005.01349.x, 2005.

Fuhrer, J., Skärby, L. and Ashmore, M.R.: Critical levels for ozone effects on vegetation in Europe, Environ. Pollut., 97, 91-106, https://doi.org/10.1016/S0269-7491(97)00067-5, 1997.

Gong, C., Lei, Y., Ma, Y., Yue, X., and Liao, H.: Ozone–vegetation feedback through

dry deposition and isoprene emissions in a global chemistry–carbon–climate model, Atmos. Chem. Phys., 20, 3841–3857, https://doi.org/10.5194/acp-20-3841-2020, 2020.

Gregg, J. W., Jones, C. G., and Dawson, T. E.: Physiological and Developmental Effects of O_3 on Cottonwood Growth in Urban and Rural Sites, Ecol. Appl., 16, 2368–2381, https://doi.org/10.1890/1051-0761(2006)016[2368:PADEOO]2.0.CO;2, 2006.

Hoesly, R. M., Smith, S. J., Feng, L., Klimont, Z., Janssens-Maenhout, G., Pitkanen, T., Seibert, J. J., Vu, L., Andres, R. J., Bolt, R. M., Bond, T. C., Dawidowski, L., Kholod, N., Kurokawa, J., Li, M., Liu, L., Lu, Z., Moura, M. C. P., O'Rourke, P. R., and Zhang, Q.: Historical (1750–2014) anthropogenic emissions of reactive gases and aerosols from the Community Emissions Data System (CEDS), Geosci. Model. Dev., 11, 369–408, https://doi.org/10.5194/gmd-11-369-2018, 2018.

Huffman, G. J., Adler, R. F., Arkin, P., Chang, A., Ferraro, R., Gruber, A., Janowiak, J., McNab, A., Rudolf, B., and Schneider, U.: The Global Precipitation Climatology Project (GPCP) Combined Precipitation Dataset, B. Am. Meteorol. Soc., 78, 5–20, https://doi.org/10.1175/1520-0477(1997)078<0005:TGPCPG>2.0.CO;2, 1997.

Hurtt, G. C., Chini, L., Sahajpal, R., Frolking, S., Bodirsky, B. L., Calvin, K., Doelman, J. C., Fisk, J., Fujimori, S., Klein Goldewijk, K., Hasegawa, T., Havlik, P., Heinimann, A., Humpenöder, F., Jungclaus, J., Kaplan, J. O., Kennedy, J., Krisztin, T., Lawrence, D., Lawrence, P., Ma, L., Mertz, O., Pongratz, J., Popp, A., Poulter, B., Riahi, K., Shevliakova, E., Stehfest, E., Thornton, P., Tubiello, F. N., van Vuuren, D. P., and Zhang, X.: Harmonization of global land use change and management for the period 850–2100 (LUH2) for CMIP6, Geosci. Model. Dev., 13, 5425–5464, https://doi.org/10.5194/gmd-13-5425-2020, 2020.

Ito, G., Romanou, A., Kiang, N.Y., Faluvegi, G., Aleinov, I., Ruedy, R., Russell, G., Lerner, P., Kelley, M. and Lo, K.: Global carbon cycle and climate feedbacks in the NASA GISS ModelE2, J. Adv. Model. Earth. Sy., 12, https://doi.org/10.1029/2019MS002030, 2020.

Jin, Z., Yan, D., Zhang, Z., Li, M., Wang, T., Huang, X., Xie, M., Li, S., and Zhuang, B.: Effects of Elevated Ozone Exposure on Regional Meteorology and Air Quality in China Through Ozone-Vegetation Coupling, J. Geophys. Res-Atmos., 128, e2022JD038119, https://doi.org/10.1029/2022JD038119, 2023.

Jolivet, Y., Bagard, M., Cabané, M., Vaultier, M.-N., Gandin, A., Afif, D., Dizengremel, P., and Le Thiec, D.: Deciphering the ozone-induced changes in cellular processes: a prerequisite for ozone risk assessment at the tree and forest levels, Ann. For. Sci., 73, 923–943, https://doi.org/10.1007/s13595-016-0580-3, 2016.

Jung, M., Reichstein, M., Margolis, H.A., Cescatti, A., Richardson, A.D., Arain, M.A.,

Arneth, A., Bernhofer, C., Bonal, D., Chen, J. and Gianelle, D.: Global patterns of land-atmosphere fluxes of carbon dioxide, latent heat, and sensible heat derived from eddy covariance, satellite, and meteorological observations. J. Geophys. Res-Biogeosci., 116(G3), https://doi.org/10.1029/2010JG001566, 2011.

Kalnay, E., Kanamitsu, M., Kistler, R., Collins, W., Deaven, D., Gandin, L., Iredell, M., Saha, S., White, G., Woollen, J., Zhu, Y., Chelliah, M., Ebisuzaki, W., Higgins, W., Janowiak, J., Mo, K. C., Ropelewski, C., Wang, J., Leetmaa, A., Reynolds, R., Jenne, R., and Joseph, D.: The NCEP/NCAR 40-Year Reanalysis Project, B. Am. Meteorol. Soc., 77, 437–472, https://doi.org/10.1175/1520-0477(1996)077<0437:TNYRP>2.0.CO;2, 1996.

Karlsson, P., Uddling, J., Braun, S., Broadmeadow, M., Elvira, S., Gimeno, B., Le Thiec, D., Oksanen, E., Vandermeiren, K., Wilkinson, M., and Emberson, L.: New critical levels for ozone effects on young trees based on AOT40 and simulated cumulative leaf uptake of ozone, Atmos. Environ., 38, 2283–2294, https://doi.org/10.1016/j.atmosenv.2004.01.027, 2004.

Koch, D., Schmidt, G. A., and Field, C. V.: Sulfur, sea salt, and radionuclide aerosols in GISS ModelE, J. Geophys. Res-Atmos, 111, https://doi.org/10.1029/2004JD005550, 2006.

Laisk, A., Kull, O., & Moldau, H.: Ozone concentration in leaf intercellular air spaces is close to zero. Plant Physiol., 90(3), 1163-1167, https://doi.org/10.1104/pp.90.3.1163, 1989.

Lam, J. C. Y., Tai, A. P. K., Ducker, J. A., and Holmes, C. D.: Development of an ecophysiology module in the GEOS-Chem chemical transport model version 12.2.0 to represent biosphere–atmosphere fluxes relevant for ozone air quality, Geosci. Model. Dev., 16, 2323–2342, https://doi.org/10.5194/gmd-16-2323-2023, 2023.

Lei, Y., Yue, X., Liao, H., Gong, C., and Zhang, L.: Implementation of Yale Interactive terrestrial Biosphere model v1.0 into GEOS-Chem v12.0.0: a tool for biosphere–chemistry interactions, Geosci. Model. Dev., 13, 1137–1153, https://doi.org/10.5194/gmd-13-1137-2020, 2020.

Lei, Y., Yue, X., Liao, H., Zhang, L., Yang, Y., Zhou, H., Tian, C., Gong, C., Ma, Y., and Gao, L.: Indirect contributions of global fires to surface ozone through ozone–vegetation feedback, Atmos. Chem. Phys., 21, 11531–11543, https://doi.org/10.5194/acp-21-11531-2021, 2021.

Li, Y., Henze, D.K., Jack, D.: The influence of air quality model resolution on health impact assessment for fine particulate matter and its components, Air. Qual. Atmos. Hlth., 9, 51-68, https://doi.org/10.1007/s11869-015-0321-z, 2016.

Lin, M., Horowitz, L.W., Xie, Y., Paulot, F., Malyshev, S., Shevliakova, E., Finco, A., Gerosa, G., Kubistin, D. and Pilegaard, K.: Vegetation feedbacks during drought exacerbate ozone air pollution extremes in Europe, Nat. Clim. Change., 10,444-451, https://doi.org/10.1038/s41558-020-0743-y, 2020.

Lombardozzi, D., Levis, S., Bonan, G., and Sparks, J. P.: Predicting photosynthesis and transpiration responses to ozone: decoupling modeled photosynthesis and stomatal conductance, Biogeosciences, 9, 3113–3130, https://doi.org/10.5194/bg-9-3113-2012, 2012.

Lombardozzi, D., Sparks, J. P., and Bonan, G.: Integrating O_3 influences on terrestrial processes: photosynthetic and stomatal response data available for regional and global modeling, Biogeosciences, 10, 6815–6831, https://doi.org/10.5194/bg-10-6815-2013, 2013.

Lombardozzi, D., Levis, S., Bonan, G., Hess, P. G., and Sparks, J. P.: The Influence of Chronic Ozone Exposure on Global Carbon and Water Cycles, J. Climate., 28, 292–305, https://doi.org/10.1175/JCLI-D-14-00223.1, 2015.

van Marle, M. J. E., Kloster, S., Magi, B. I., Marlon, J. R., Daniau, A.-L., Field, R. D., Arneth, A., Forrest, M., Hantson, S., Kehrwald, N. M., Knorr, W., Lasslop, G., Li, F., Mangeon, S., Yue, C., Kaiser, J. W., and van der Werf, G. R.: Historic global biomass burning emissions for CMIP6 (BB4CMIP) based on merging satellite observations with proxies and fire models (1750–2015), Geosci. Model. Dev., 10, 3329–3357, https://doi.org/10.5194/gmd-10-3329-2017, 2017.

Menon, S. and Rotstayn, L.: The radiative influence of aerosol effects on liquid-phase cumulus and stratiform clouds based on sensitivity studies with two climate models, Clim. Dyn., 27, 345–356, https://doi.org/10.1007/s00382-006-0139-3, 2006.

Mills, G., Buse, A., Gimeno, B., Bermejo, V., Holland, M., Emberson, L., and Pleijel, H.: A synthesis of AOT40-based response functions and critical levels of ozone for agricultural and horticultural crops, Atmos. Environ., 41, 2630–2643, https://doi.org/10.1016/j.atmosenv.2006.11.016 , 2007.

Mills, G., Harmens, H., Wagg, S., Sharps, K., Hayes, F., Fowler, D., Sutton, M. and Davies, B.: Ozone impacts on vegetation in a nitrogen enriched and changing climate, Environ. Pollut., 208, 898-908, https://doi.org/10.1016/j.envpol.2015.09.038, 2016.

Myhre, G., Shindell, D., Breìon, F.-M., Collins, W., Fuglestvedt, J., Huang, J., Koch, D., Lamarque, J.-F., Lee, D., Mendoza, B., Nakajima, T., Robock, A., Stephens, G., Takemura, T., and Zhang, H., Anthropogenic and Natural Radiative Forcing, in: Climate Change 2013: The Physical Science Basis. Contribution of Working Group I to the Fifth Assessment Report of the Intergovernmental Panel on Climate

671 Change, edited by: Stocker, T. F., Qin, D., Plattner, G.-K., Tignor, M., Allen, S. K.,
672 Boschung, J., Nauels, A., Xia, Y., Bex, V., and Midgley, P. M., Cambridge
673 University Press, Cambridge, UK and New York, NY, USA, 2013.

674 Norval, M., Lucas, R. M., Cullen, A. P., De Gruijl, F. R., Longstreth, J., Takizawa, Y.,
675 and Van Der Leun, J. C.: The human health effects of ozone depletion and
676 interactions with climate change, Photoch. Photobio. Sci., 10, 199–225,
677 https://doi.org/10.1039/C0PP90044C, 2011.

678 Nussbaum, S. and Fuhrer, J.: Difference in ozone uptake in grassland species between
679 open-top chambers and ambient air, Environ. Pollut., 109, 463–471,
680 https://doi.org/10.1016/S0269-7491(00)00049-X, 2000.

681 Nuvolone, D., Petri, D., and Voller, F.: The effects of ozone on human health, Environ.
682 Sci. Pollut. R., 25, 8074–8088, https://doi.org/10.1007/s11356-017-9239-3, 2018.

683 Ohara, T., Akimoto, H., Kurokawa, J., Horii, N., Yamaji, K., Yan, X., and Hayasaka, T.:
684 An Asian emission inventory of anthropogenic emission sources for the period
685 1980-2020, Atmos. Chem. Phys., 7, 4419–4444, https://doi.org/10.5194/acp-7-
686 4419-2007, 2007.

687 Oleson, K. W., Lawrence, D. M., Bonan, G. B., Flanne, M. G., Kluzek, E., Lawrence,
688 P. J., Levis, S., Swenson, S. C., and Thornton, P. E.: Technical Description of
689 version 4.0 of the Community Land Model (CLM), National Center for
690 Atmospheric Research, Boulder, USA, CONCAR/TN-478+STR, 2010.

691 Oliver, R. J., Mercado, L. M., Sitch, S., Simpson, D., Medlyn, B. E., Lin, Y.-S., and
692 Folberth, G. A.: Large but decreasing effect of ozone on the European carbon sink,
693 Biogeosciences, 15, 4245–4269, 2018.

694 Petters, M. D. and Kreidenweis, S. M.: A single parameter representation of
695 hygroscopic growth and cloud condensation nucleus activity, Atmos. Chem. Phys.,
696 7, 1961–1971, https://doi.org/10.5194/acp-7-1961-2007, 2007.

697 Paoletti, E., De Marco, A. and Racalbuto, S.: Why should we calculate complex indices
698 of ozone exposure? Results from Mediterranean background sites. Environ. Monit.
699 Assess., 128, pp.19-30, https://doi.org/10.1007/s10661-006-9412-5, 2007.

700 Pitchford, M., Malm, W., Schichtel, B., Kumar, N., Lowenthal, D., and Hand, J.:
701 Revised Algorithm for Estimating Light Extinction from IMPROVE Particle
702 Speciation Data, Japca. J. Air. Waste. Ma., 57 (11), 1326–1336,
703 https://doi.org/10.3155/1047-3289.57.11.1326, 2007.

704 Pleijel, H., Danielsson, H., Ojanperä, K., Temmerman, L. D., Högy, P., Badiani, M.,
705 and Karlsson, P. E.: Relationships between ozone exposure and yield loss in
706 European wheat and potato—a comparison of concentration- and flux-based
707 exposure indices, Atmos. Environ., 38, 2259–2269,

https://doi.org/10.1016/j.atmosenv.2003.09.076, 2004.

Pleijel, H., Danielsson, H., Emberson, L., Ashmore, M. R., and Mills, G.: Ozone risk assessment for agricultural crops in Europe: further development of stomatal flux and flux–response relationships for European wheat and potato, Atmos. Environ., 41, 3022–3040, https://doi.org/10.1016/j.atmosenv.2006.12.002, 2007.

Remer, L. A., Kaufman, Y. J., Tanré, D., Mattoo, S., Chu, D. A., Martins, J. V., Li, R.-R., Ichoku, C., Levy, R. C., and Kleidman, R. G.: The MODIS aerosol algorithm, products, and validation, J. Atmos. Sci., 62, 947–973, https://doi.org/10.1175/JAS3385.1, 2005.

Sadiq, M., Tai, A. P., Lombardozzi, D., and Val Martin, M.: Effects of ozone–vegetation coupling on surface ozone air quality via biogeochemical and meteorological feedbacks, Atmos. Chem. Phys., 17, 3055–3066, https://doi.org/10.5194/acp-17-3055-2017, 2017.

Schmidt, G. A., Ruedy, R., Hansen, J. E., Aleinov, I., Bell, N., Bauer, M., Bauer, S., Cairns, B., Canuto, V., Cheng, Y., Genio, A. D., Faluvegi, G., Friend, A. D., Hall, T. M., Hu, Y., Kelley, M., Kiang, N. Y., Koch, D., Lacis, A. A., Lerner, J., Lo, K. K., Miller, R. L., Nazarenko, L., Oinas, V., Perlwitz, J., Perlwitz, J., Rind, D., Romanou, A., Russell, G. L., Sato, M., Shindell, D. T., Stone, P. H., Sun, S., Tausnev, N., Thresher, D., and Yao, M.-S.: Present-Day Atmospheric Simulations Using GISS ModelE: Comparison to In Situ, Satellite, and Reanalysis Data, J. Climate., 19, 153–192, https://doi.org/10.1175/JCLI3612.1, 2006.

Schmidt, G. A., Kelley, M., Nazarenko, L., Ruedy, R., Russell, G. L., Aleinov, I., Bauer, M., Bauer, S. E., Bhat, M. K., Bleck, R., Canuto, V., Chen, Y.-H., Cheng, Y., Clune, T. L., Del Genio, A., de Fainchtein, R., Faluvegi, G., Hansen, J. E., Healy, R. J., Kiang, N. Y., Koch, D., Lacis, A. A., LeGrande, A. N., Lerner, J., Lo, K. K., Matthews, E. E., Menon, S., Miller, R. L., Oinas, V., Oloso, A. O., Perlwitz, J. P., Puma, M. J., Putman, W. M., Rind, D., Romanou, A., Sato, M., Shindell, D. T., Sun, S., Syed, R. A., Tausnev, N., Tsigaridis, K., Unger, N., Voulgarakis, A., Yao, M.-S., and Zhang, J.: Configuration and assessment of the GISS ModelE2 contributions to the CMIP5 archive: GISS MODEL-E2 CMIP5 SIMULATIONS, J. Adv. Model. Earth Syst., 6, 141–184, https://doi.org/10.1002/2013MS000265, 2014.

Sicard, P., De Marco, A., Dalstein-Richier, L., Tagliaferro, F., Renou, C., Paoletti, Elena, 2016. An epidemiological assessment of stomatal ozone flux-based critical levels for visible ozone injury in southern European forests. Sci. Total. Environ., 541, 729-741.

Sitch, S., Cox, P. M., Collins, W. J., and Huntingford, C.: Indirect radiative forcing of climate change through ozone effects on the land-carbon sink, Nature, 448, 791–794, https://doi.org/10.1038/nature06059, 2007.

747 Sofen, E. D., Bowdalo, D., Evans, M. J., Apadula, F., Bonasoni, P., Cupeiro, M., Ellul,
748 R., Galbally, I. E., Girgzdiene, R., Luppo, S., Mimouni, M., Nahas, A. C., Saliba,
749 M., and Tørseth, K.: Gridded global surface ozone metrics for atmospheric
750 chemistry model evaluation, Earth Syst. Sci. Data, 8, 41–59,
751 https://doi.org/10.5194/essd-8-41-2016, 2016.

752 Unger, N., Zheng, Y., Yue, X., and Harper, K. L.: Mitigation of ozone damage to the
753 world's land ecosystems by source sector, Nat. Clim. Chang., 10, 134–137,
754 https://doi.org/10.1038/s41558-019-0678-3, 2020.

755 VanLoocke, A., Betzelberger, A. M., Ainsworth, E. A., and Bernacchi, C. J.: Rising
756 ozone concentrations decrease soybean evapotranspiration and water use
757 efficiency whilst increasing canopy temperature, New. Phytol., 195, 164–171,
758 https://doi.org/10.1111/j.1469-8137.2012.04152.x, 2012.

759 van der Werf, G. R., Randerson, J. T., Giglio, L., van Leeuwen, T. T., Chen, Y., Rogers,
760 B. M., Mu, M., van Marle, M. J. E., Morton, D. C., Collatz, G. J., Yokelson, R. J.,
761 and Kasibhatla, P. S.: Global fire emissions estimates during 1997–2016, Earth.
762 Syst. Sci. Data, 9, 697–720, https://doi.org/10.5194/essd-9-697-2017, 2017.

763 Wang, Y., Shen, L., Wu, S., Mickley, L., He, J. and Hao, J.: Sensitivity of surface ozone
764 over China to 2000–2050 global changes of climate and emissions, Atmos.
765 Environ, 75, 374-382, https://doi.org/10.1016/j.atmosenv.2013.04.045, 2013.

766 Wesely, M. L. and Hicks, B. B.: A review of the current status of knowledge on dry
767 deposition, Atmos. Environ., 34, 2261–2282, https://doi.org/10.1016/S1352-
768 2310(99)00467-7, 2000.

769 Wild, M., Folini, D., Schär, C., Loeb, N., Dutton, E. G., and König-Langlo, G.: The
770 global energy balance from a surface perspective, Clim. Dyn., 40, 3107–3134,
771 https://doi.org/10.1007/s00382-012-1569-8, 2013.

772 Yue, X., Liao, H., Wang, H. J., Li, S. L., and Tang, J. P.: Role of sea surface temperature
773 responses in simulation of the climatic effect of mineral dust aerosol, Atmos.
774 Chem. Phys., 11, 6049-6062, https://doi.org/10.5194/acp-11-6049-2011, 2011.

775 Yue, X. and Unger, N.: Ozone vegetation damage effects on gross primary productivity
776 in the United States, Atmos. Chem. Phys., 14, 9137–9153,
777 https://doi.org/10.5194/acp-14-9137-2014, 2014.

778 Yue, X. and Unger, N.: The Yale Interactive terrestrial Biosphere model version 1.0:
779 description, evaluation and implementation into NASA GISS ModelE2, Geosci.
780 Model Dev., 8, 2399–2417, https://doi.org/10.5194/gmd-8-2399-2015, 2015.

781 Yue, X. and Unger, N.: Fire air pollution reduces global terrestrial productivity, Nat.
782 Commun., 9, 5413, https://doi.org/10.1038/s41467-018-07921-4, 2018.

Yue, X., Keenan, T. F., Munger, W., and Unger, N.: Limited effect of ozone reductions on the 20-year photosynthesis trend at Harvard forest, Glob. Change Biol., 22, 3750–3759, https://doi.org/10.1111/gcb.13300, 2016.

Yue, X., Liao, H., Wang, H., Zhang, T., Unger, N., Sitch, S., Feng, Z., and Yang, J.: Pathway dependence of ecosystem responses in China to 1.5°C global warming, Atmos. Chem. Phys., 20, 2353–2366, https://doi.org/10.5194/acp-20-2353-2020, 2020.

Zhang, L., Vet, R., Brook, J. R., and Legge, A. H.: Factors affecting stomatal uptake of ozone by different canopies and a comparison between dose and exposure, Sci. Total Environ., 370, 117–132, https://doi.org/10.1016/j.scitotenv.2006.06.004, 2006.

Zhou, X., Yue, X., and Tian, C.: Responses of Ecosystem Productivity to Anthropogenic Ozone and Aerosols at the 2060, Earths Future, 12, e2023EF003781, https://doi.org/10.1029/2023EF003781, 2024.

Zhu, J., Tai, A. P. K., and Hung Lam Yim, S.: Effects of ozone–vegetation interactions on meteorology and air quality in China using a two-way coupled land–atmosphere model, Atmos. Chem. Phys., 22, 765–782, https://doi.org/10.5194/acp-22-765-2022, 2022.